

Solar flare induced cosmic noise absorption

Olugbenga Ogunmodimu ¹ formerly at ², Farideh Honary ², Neil Rogers ², E.O Falayi ³, and

O.S Bolaji ⁴

1. Centre for Atmospheric Research, National Space Research and Development Agency of Nigeria, (NASRDA).
2. Physics Department, Lancaster University, Lancaster, United Kingdom
3. Department of Physics, Tai Solarin University of Education, Ijagun, P.M.B 2118, Ijebu Ode, Ogun State, Nigeria
4. Physics Department, University of Lagos, Akoka, Lagos Nigeria.

Abstract

Solar flare events are a major observing emphasis for space weather because they affect the ionosphere and can eject high-energy particles that can adversely affect Earth's technologies. In this study we model 38.2 MHz cosmic noise absorption (CNA) by utilising measurements from the Imaging Riometer for Ionospheric Studies (IRIS) at Kilpisjärvi, Finland obtained during solar cycle 23 (1996-2009). We utilised X-ray archive for the same period from the Geostationary Operational Environmental Satellite (GOES) to study solar flare induced cosmic noise absorption. We identified the threshold of flare (M4 class) that could bear significant influence on CNA. Through epoch analysis, we show the magnitude of absorption that each class of flare could produce. Using the parameters of flare and absorption we present a model that could provide the basis for nowcast of CNA induced by M and X-class solar flares.

1.0 Introduction

Radio waves passing through an ionised medium cause the electrons to vibrate. If these electrons collide with heavy particles, energy is transferred from the wave to the medium in the form of plasma thermal energy and the rate of wave attenuation is then dependent on the number of collisions per oscillation. The electron density, the gyro frequency, and the electron collisions with neutral atoms and molecules affect the passage of radio waves through the ionosphere [e.g. Schunk and Nagy 2009, Hargreaves 1995, Takanama et al, 2007]. Cosmic radio noise refers to the background radio frequency radiation from galactic sources, having constant intensity during geomagnetically quiet periods. The cosmic noise intensity measured with ground-based receivers will fluctuate corresponding to the level of ionisation in the earth's ionosphere. Increased ionisation results in absorption of the cosmic radio noise as it passes through the ionosphere. Comparing the noise level recorded by ground-based equipment such as riometers with the expected value in the absence of the ionospheric absorption, the level of absorption can be computed from:

Where A is absorption in decibel, p is the measured noise level and p_0 is the noise level measured in the absence of absorption [Browne et al, 1995].

Solar flares are sudden explosive releases of stored magnetic energy in the atmosphere of the Sun causing sudden brightening of the photosphere which can last from few minutes to several hours [Keith, 1991]. During solar flare events, particles and electromagnetic emissions can affect the Earth's atmosphere. The three phases of flare events are the pre-flare phase, the rise phase and the main phase. The pre-flare phase is characterised by slowly rising prominence on the solar surface due to some weak eruptive instability. Normally, this phase lasts for half an hour and is accompanied by X-ray brightening. During the rise phase, the stretched magnetic field lines start to break and reconnect; in the process, prominences erupt more quickly with a steep rise in $H\alpha$ and soft X-ray emissions. During the main phase, the reconnection point rises, hot X-ray loops and $H\alpha$ ribbons are created [e.g. Hudson, 2000]. The explosive release that accompanies flare event leads to the emission of ultraviolet (UV) and X-ray radiation and can drive energetic particle precipitation. At the time of the flare, the ionisation of the D region of the dayside ionosphere can increase [e.g. Stauning, 1996], resulting in the so-called 'Sudden Ionospheric Disturbances' (SIDs), and the associated absorption is known as sudden cosmic noise absorption (SCNA). Nwankwo et al (2016) identified merits in studying sudden ionospheric disturbances related to prompt X-ray flux output from solar flares.

The duration of SCNA absorption is usually of the order of the flare [Stauning, 1996; Longden, 2007]. Figure 1 below shows the incident power and absorption plots from the central beam of IRIS riometer at Kilpisjärvi during the solar flare of 7th July, 2000. SCNA is observed following apparent increase in the received noise power. The increase of received power is attributable to an increase in the solar radio emission at the time of the flare. During intense SIDs there can be considerable disruption and even blackouts to radio communications, particularly at the higher latitudes as a result of absorption in the D and lower E regions. Previous studies [e.g. Hultqvist et al., 1999 and Contreira, 2004] associated the flare process to magnetic reconnection within the solar corona in which processed magnetic energy is converted to thermal energy and particles are accelerated. The frequency and intensity of flares is known to depend on the solar cycle with more events occurring during solar maximum.

Changes in the electromagnetic spectrum have been monitored in the x-ray monitoring devices installed in satellites; an archive of hard and soft x-ray measurement is detailed in the National Oceanic and Atmospheric Administration (NOAA) archive. In the archive, flare events are classified based on intensity (See Table 1). Solar flares are classified by their x-ray flux in the 1.0 - 8.0 Angstrom band as measured by the NOAA GOES-8 and GOES12-15 satellite. This paper aims to provide an empirical basis for a nowcast of cosmic noise absorption induced by M and X class flares. X-ray solar flux data used in this work is from the Geostationary Operational Environmental Satellite (GOES)

(<http://www.ngdc.noaa.gov/stp/space-weather/solar-data/solar-features/solar-flares/>), the x-ray and CNA data utilized covers solar cycle 23 (1996-2009).

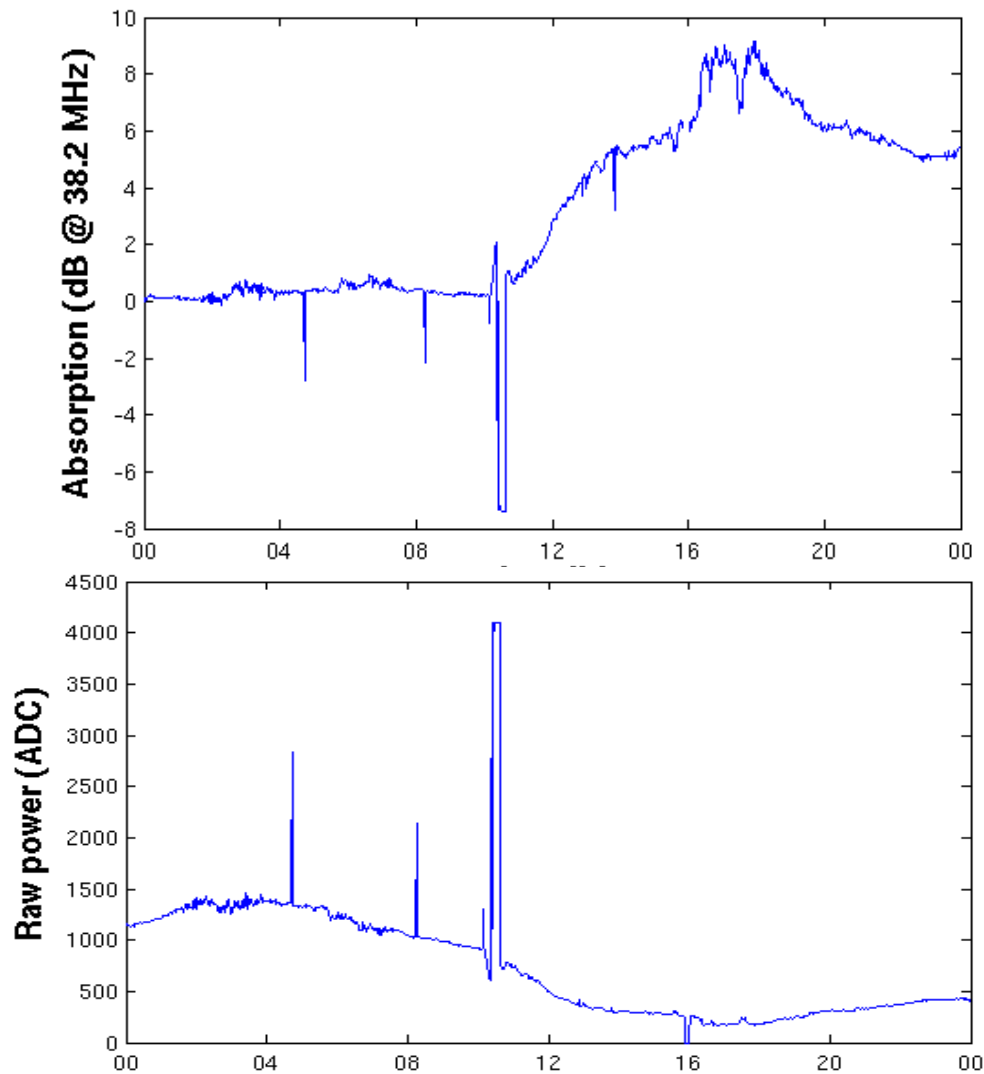


Figure 1: Figure 6.1: Cosmic noise absorption event following solar flare of 14th July, 2000. Panel (a) shows the derived cosmic noise absorption from incident power on the y-axis and local time variation on

the x-axis. Panel (b) shows incident cosmic noise power detected by central beam (beam 25) of IRIS at Kilpisjärvi, Finland, 69.05 deg N, 20.79 deg E) the x-axis shows local time variation. The arrow on panel (b) shows the time of commencement of the X-class flare just after 10:24UT, gradual increase in riometer absorption began just after 10:24UT from about 0.2dB up to 8dB at 17:00 hours.

2.0 Data and Instrumentation

Flares vary significantly in their relative intensities at different wavelengths. Table 1 shows how the Geostationary Operational Environmental Satellite (GOES) classify flares based on the peak intensity of soft X-ray flux network in the 1-8 Å spectral bands. In GOES, flares are classified as A, B, C, M, and X. Each class has a peak X-ray flux ten times greater than the preceding class.

Table 1: Classification of GOES soft X-ray flare

Classification	Peak Flux in 1-8 Å Range (Wm^{-2})
A	$x < 10^{-7}$
B	$10^{-7} \leq x < 10^{-6}$
C	$10^{-6} \leq x < 10^{-5}$
M	$10^{-5} \leq x < 10^{-4}$
X	$10^{-4} \leq x$

2.1 Riometry

The Riometer was developed as a means to regularly measure the ionospheric absorption [e.g. Bamford et al, 1999; Browne et al, 1995]. This is based upon the principle of monitoring cosmic radio noise absorption as developed by previous workers [e.g. Kavanagh et al, 2004; Stauning, 1996]. For riometry purposes, the average height of the absorbing layer is usually considered to be 90km. It operates passively by constantly monitoring the background cosmic noise from the sky. Because this method entails radio waves propagation through the ionosphere, the frequency

must be greater than the critical frequency. Measurement of the received power is accomplished by rapid switching between receiver input and a local noise source. The current passing through the noise diode is constantly altered to keep the power of the two noise sources equal. The power of the local noise source is proportional to the current passing through it. Hence, recording of the current is only required for the measurement of the antenna power [Browne et al, 1995]. The receiver works in a way that measurements are not affected by variations in the received gain.

2.2 The IRIS at Kilpisjärvi

Investigation into energetic particle precipitation has been achieved through the use of wide beam and imaging riometers [e.g. IRIS], which monitor the absorption of cosmic radio noise; a parameter that is directly related to the electron density in the D layer. The Imaging Riometer for Ionospheric Studies (IRIS) (Browne et al., 1995) is located at Kilpisjärvi in northern Finland (69.05° N, 20.79° E). It began operations in September 1994 and is operated by the Space and Planetary Physics Group of Lancaster University in collaboration with the Sodankylä Geophysical Observatory (SGO), Finland. IRIS samples the cosmic radio noise at 38.2 MHz (a protected frequency for astronomy) and consists of an imaging array and a single, wide beam riometer. The system uses 64 circularly polarized cross dipole antennas grouped in a square array and separated by half a wavelength (Figure 2).

The signals from each row of eight antennas are phased by Butler matrices and produce 49 narrow beams of width between 13° and 16° (Figure 2). The outputs are fed into 7 riometers through the use of time division switching. The whole array is sampled every second and switching is arranged so that each second is divided into 8 time slots. The eighth time slots are used to record the output from the co-located wide beam antenna.

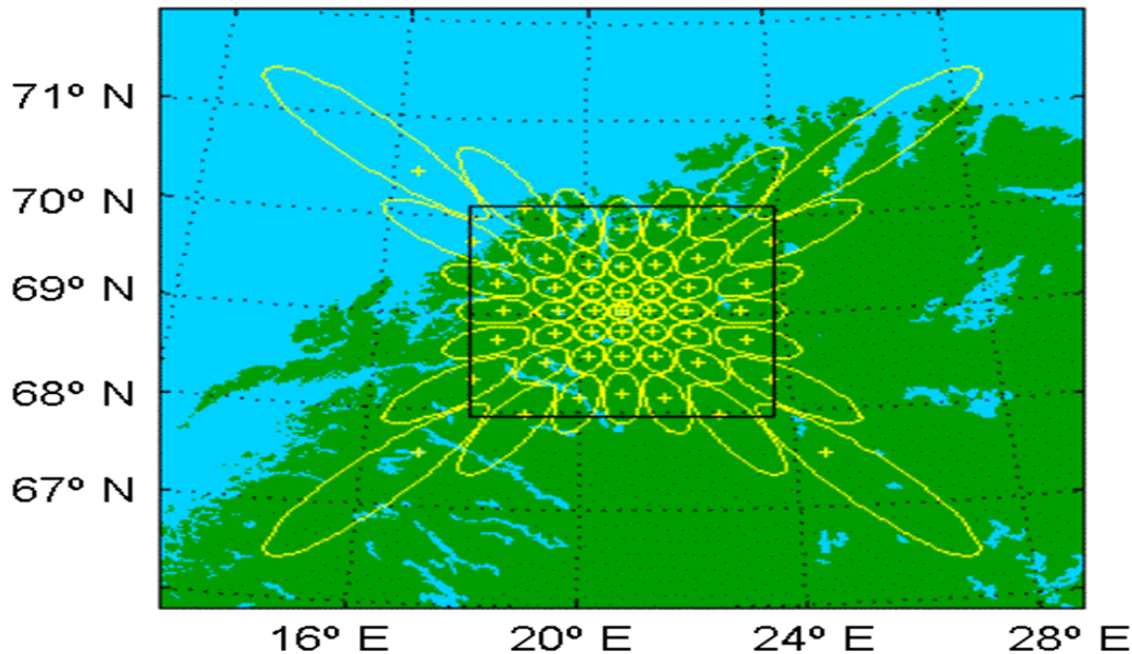


Figure 2: Beam projection of IRIS at 90 km altitude. The contours define the -3 dB points and the black square shows the calculated field of view used in the IRIS images.

Solar flare event data used in this study is from the Geostationary Operational Environmental Satellite (GOES) system. GOES began operation in 1975 with the launch of GOES-1 and provides a source of continuous solar data. The system utilises numerous satellites stationed in the geosynchronous orbits. Four satellites are currently operational GOES-12 to GOES-15. GOES-13 is designated operational East, stationed at 75°W and GOES-15 is designated operational West, stationed at 135°W . GOES-12 covers South America at 60°W and GOES-14 is in on-orbit storage at 105°W .

X-ray sensors are installed on the GOES satellites providing X-ray flux measurements with a one-minute time interval in the $0.5\text{-}4\text{\AA}$ and $1.0\text{-}8.0\text{\AA}$ spectra bands. GOES satellite can measure and record X-ray flux signature of all solar flares occurring on the Earth facing side of the Sun. This data is catalogued by the National Oceanic and Atmospheric Administration (NOAA) of the Space Weather Prediction Centre (SWPC), USA.

2.3 Flare Catalogue

All flare events reported (1996-2009) were obtained from the GOES satellites X-ray sensors in the 1-8Å spectra band. For each event, the data shows the start time, defined as the first minute in a sequence of four minutes, a steep monotonic increase in X-ray flux, the time of maximum X-ray flux and the end time defined as the time which the flux level decays to a point halfway between the maximum and pre-flare background. The data also includes the X-ray class (C1 and above as classes A and B are not recorded as a result of their high frequency and low intensity). In total the flare catalogue consists of 14,792 events, although within the analysis excluding the computation of annual flare count only 14,772 were used, this is because some events containing missing or inaccurate data were ignored. 13,203 events were C-class, 1,443 were M class and 126 events were X class flares.

3.0 Procedure and Methodology

To quantify absorption induced by M and X class solar flares, CNA data corresponding to the time of flare events were compiled. However, flare events which occurred when the Sun was below the horizon at the Riometer station would produce very little observable effects as the enhanced X-ray and UV flux produced by flares only reaches the sun facing side of the ionosphere. The flare catalogue was filtered to include only events occurring when the sun is above the horizon at the Riometer station and corresponding CNA data were obtained. For this procedure, solar declination was calculated based on the time of flare events in universal time (UT). The right ascension and declination together with the coordinates for longitude and latitude of the riometer site were used to determine the solar elevation at the specific time. We filtered events that occurred when the sun was below the horizon at the riometer station. We then utilised 1-second resolution IRIS data from beam the central beam (beam 25) from three hours before event start time to three hours after the recorded end time. This procedure reduced the total number of events to 6,020 events. 5,393 were C class, 504 were M- class and 123 are X-class flares. The effects of flare on the absorption induced by the different classes of flares were then investigated.

Flare catalogue was utilised to obtain the corresponding CNA data for each event. The one-second resolution data was converted to one-minute average to reduce scintillation in the data. The events were binned into C, M and X class and the median absorption signature computed for

each class. The median absorption signature was then used to produce flare-induced models for each class. The relationship between flare intensity and maximum corresponding absorption was investigated.

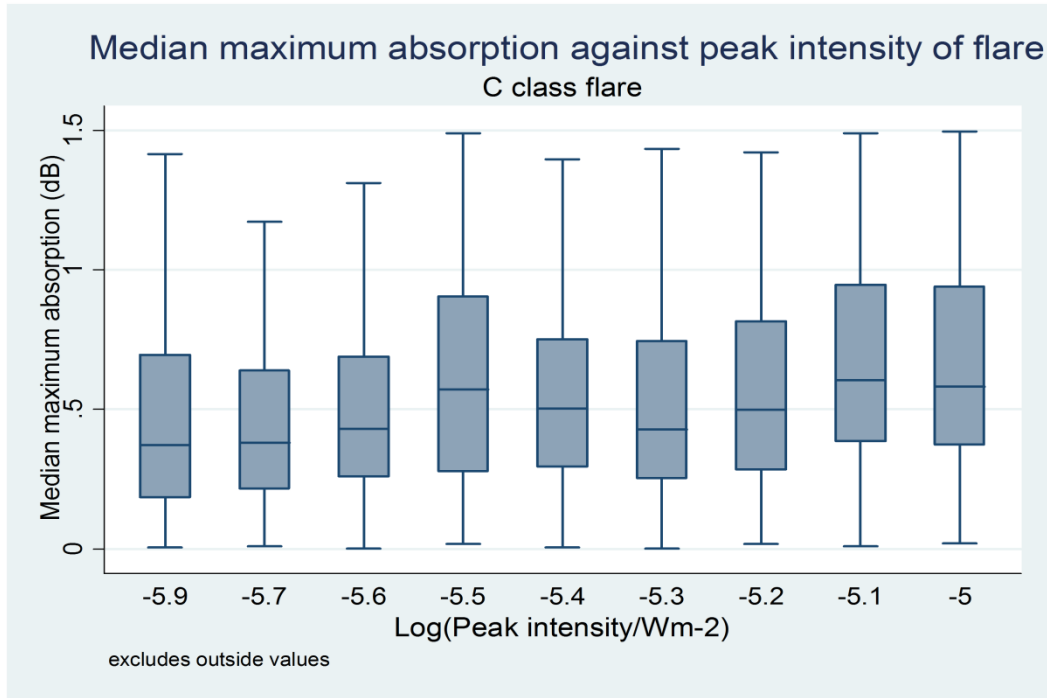


Figure 3A: Plot of median maximum absorption against log of flare intensity for C-class flares. Class (i.e. C1-C9) bins the flares and the median peak absorption computed for each bin. Here there is no visible trend in median absorption within bin classes.

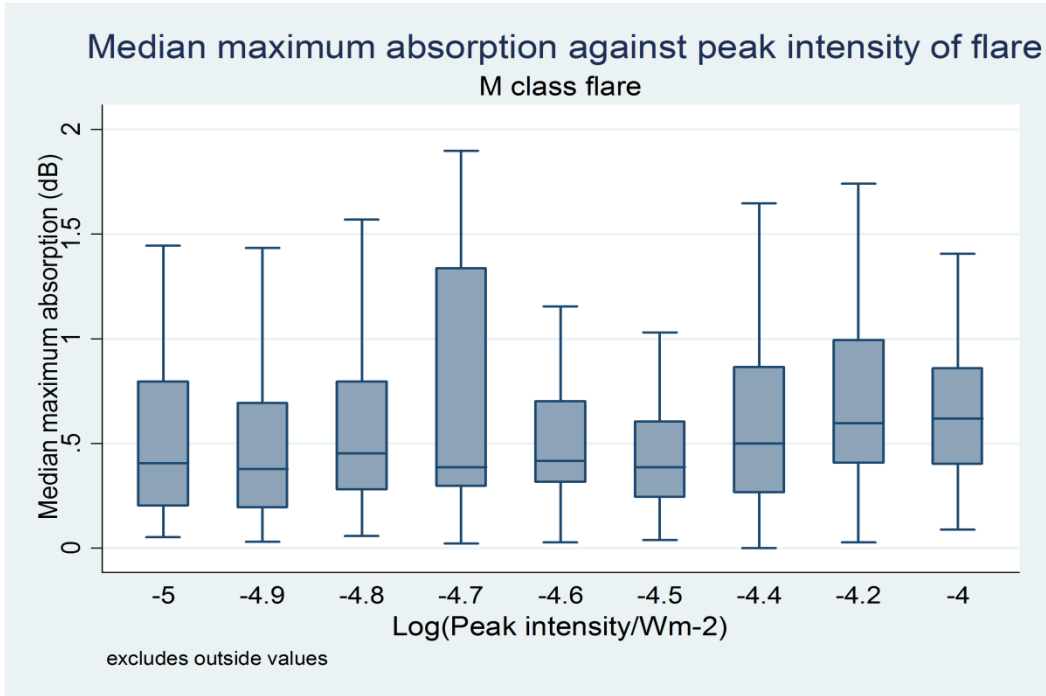


Figure 3B: Plot of median maximum absorption against log of flare intensity for M-class flares. M-class flares are binned from M1-M9 and the median peak absorption computed for each bin. No trend is observable until class M4, a gradual increase in median absorption signature within the bin from M4 to upper bin values.

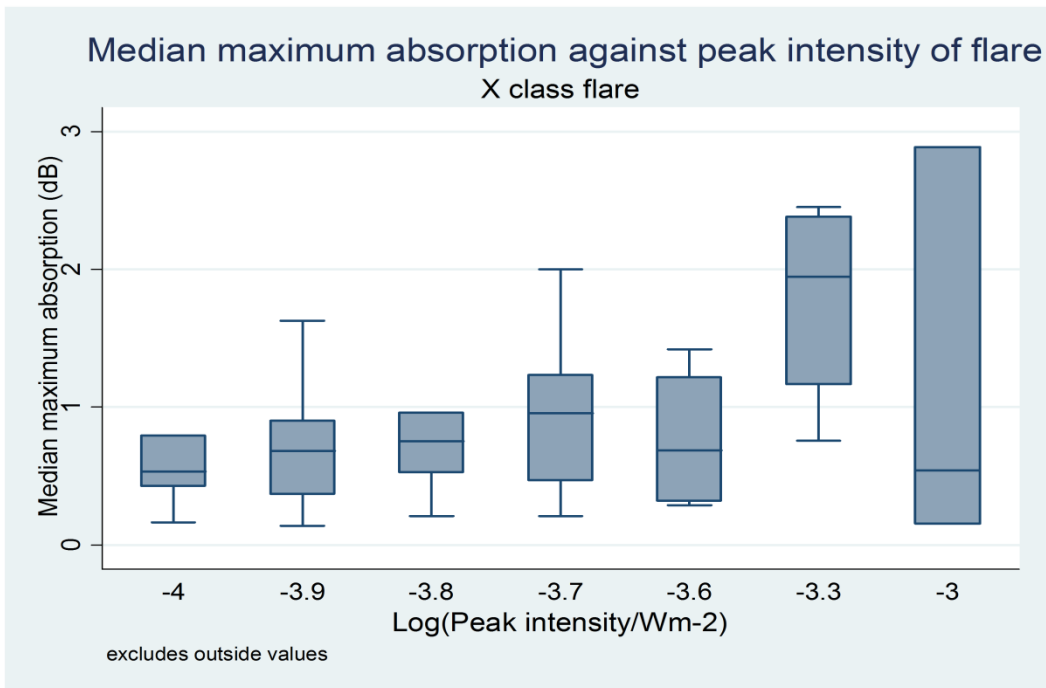


Figure 3C: Plot of median maximum absorption against log of flare intensity for X-class flares. X-class flares are binned from X1-X9 and the median peak absorption computed for each bin. There are no data in the bins X2 and X3.

Figure 3D shows the combined plot of classes C, M and X plotted against the maximum median absorption for each class.

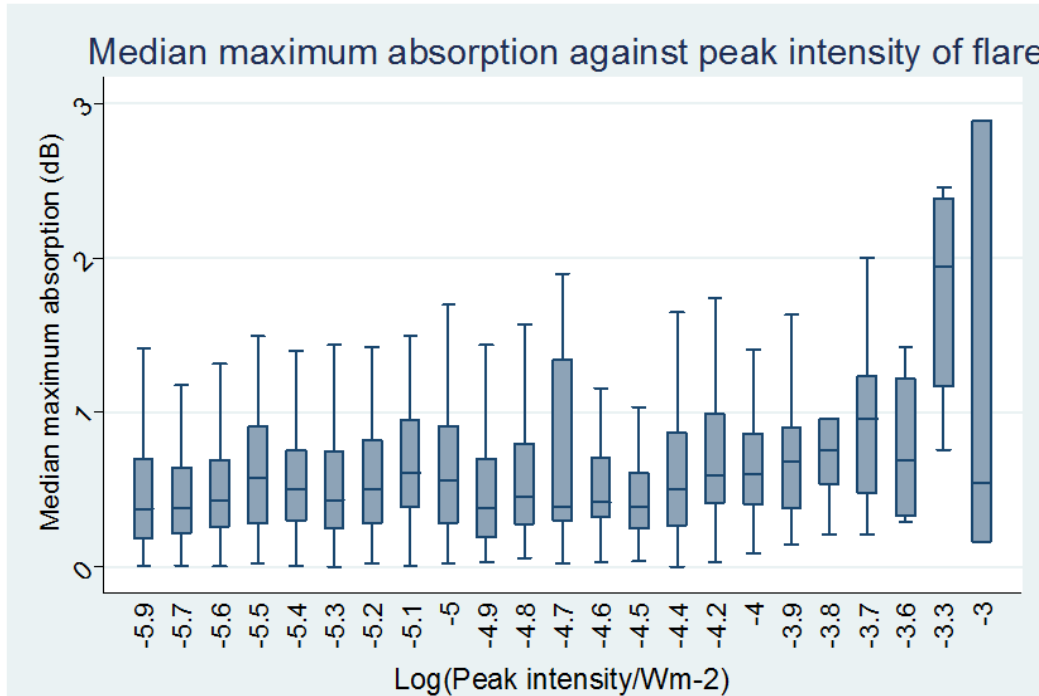


Figure 3D: Plot of median maximum absorption against Log of flare intensity for flare classes C, M and X. The flares are binned by class and plotted vs. the median peak absorption.

In Figure 3D, we show the relationship between mean duration of flare and the log of their intensity. The result shows that there appears to be no effects on absorption before the M4 flare class ($4 \times 10^{-5} \text{Wm}^{-2}$), whereas, above class M4, there is a positive correlation between maximum absorption and peak flare intensity.

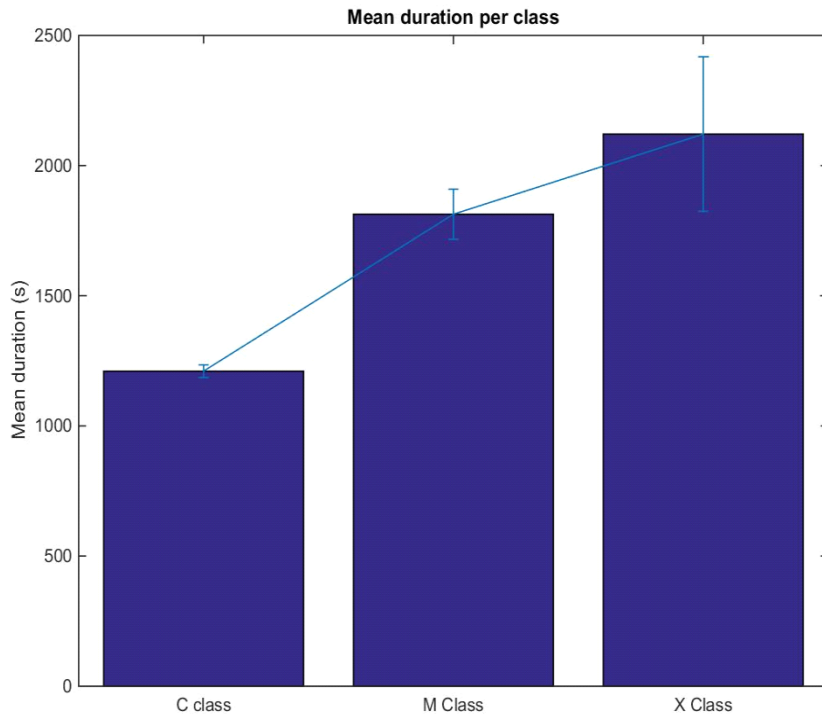


Figure 4: Plot of flare mean duration of flare for flare classes C, M and X. Flare events are binned by class and the mean duration is calculated for each. The error bar represents the standard error of the mean

In Figure 4, we show the mean duration of each flare class vary based on the intensity of each class of flare.

3.1 Epoch analysis of flare induced absorption

We show the variation of median absorption signature induced by the different classes of flare along with the first and third quartiles (Q1 and Q3). It is observed (see Figure 5) that there is no significant effect on absorption signature induced by C class fares, whereas on M class induced absorption the median signature show a deep before zero epoch (0) and a maximum after one minute and for X-class induced absorption, this will be fully discussed in section 5.

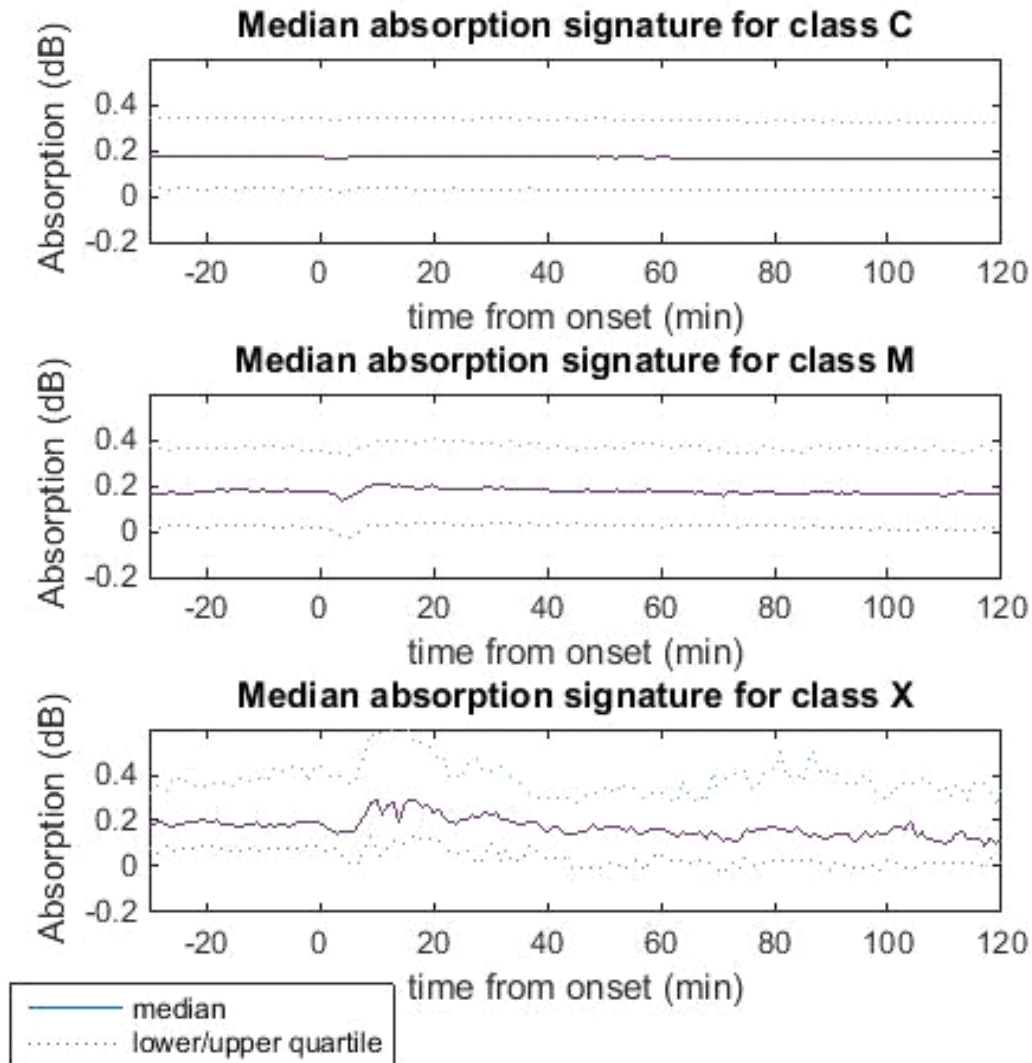


Figure 5: Superposed epoch analysis of median absorption signature for X, M and C class flare (1996-2009). The start times are as recorded by GOES. Absorption data is from beam 25 of IRIS Kilpisjarvi.

4. Model and parameterisation for flare induced absorption

Relationships between some parameters of flare events that bear corresponding effects on absorption were utilised as the building block of the flare induced absorption model. We compute the exponential rise time model of absorption and flare as well as the exponential decay time from point of maximum absorption and maximum flare intensity. The relationship between maximum absorption and maximum intensity for M and X class events were derived (Table 3).

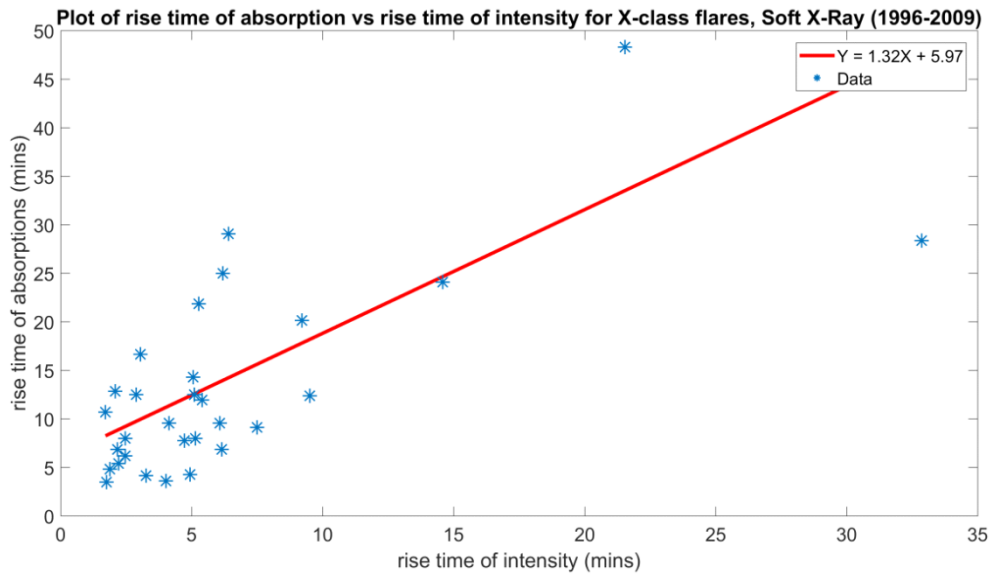
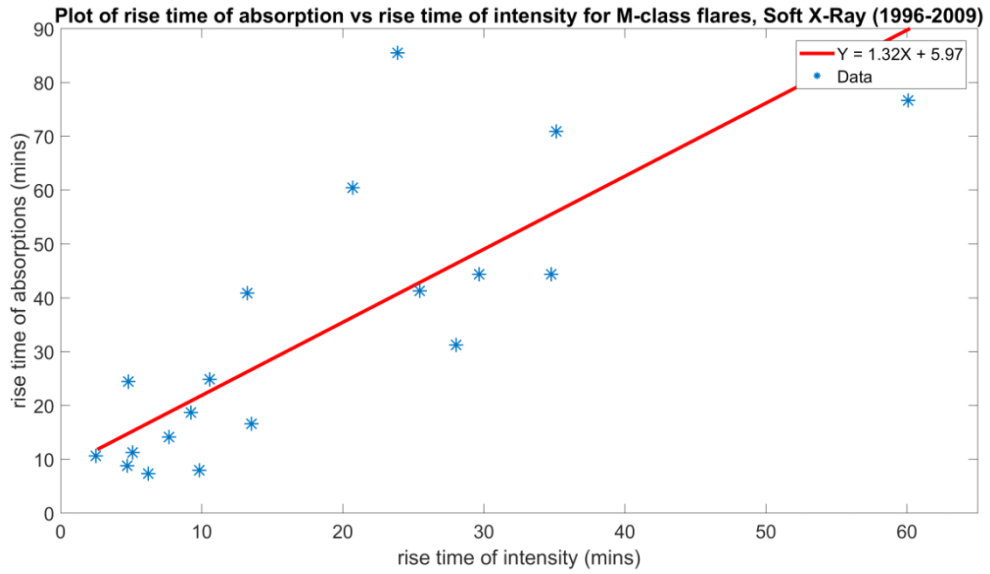


Figure 6: Plot of rise time of flare against rise time of absorption, Top panel shows rise time of M-class flare vs. rise time of absorption, bottom panel shows rise time of X-class flare vs. rise time of absorption.

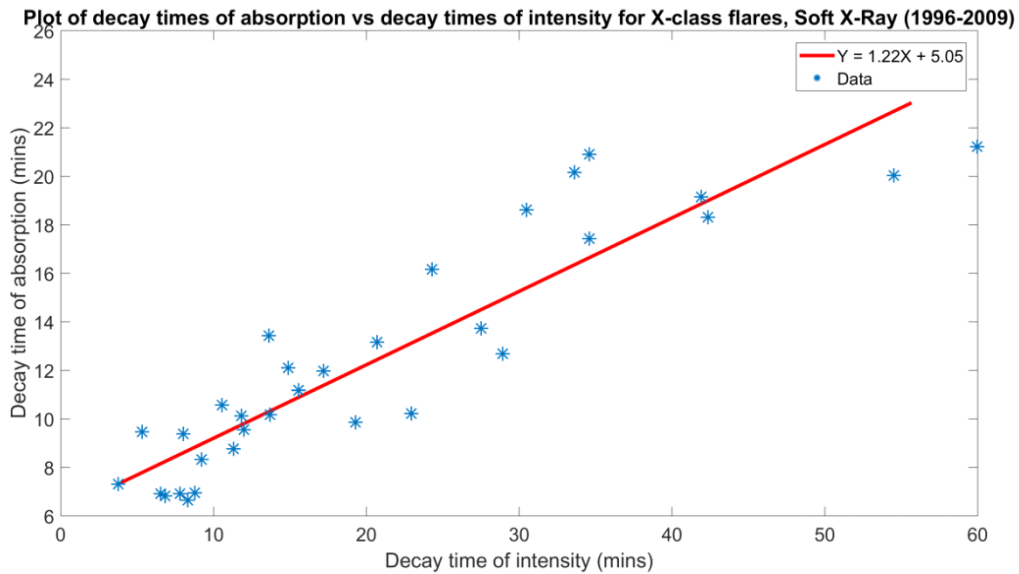
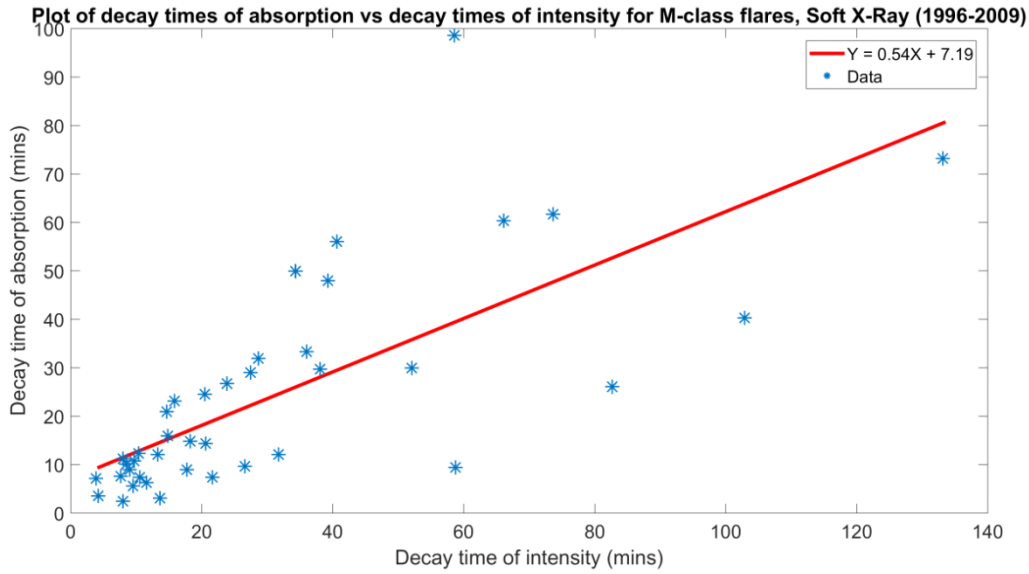


Figure 7: Plot of decay time of flare vs. decay time of absorption, top panel shows decay time of M-class flare vs. decay time in absorption. The bottom panel shows decay time in X-class flares vs. decay time in absorption,

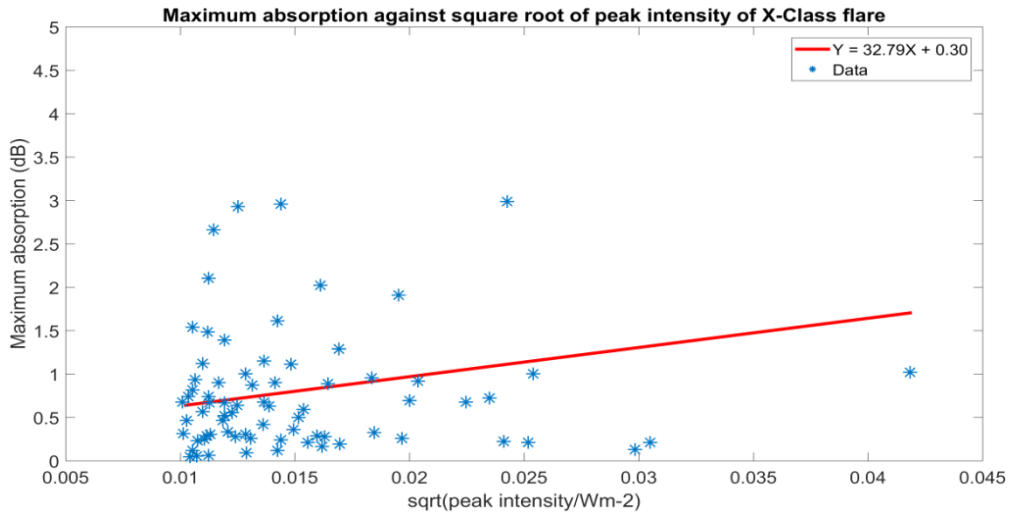
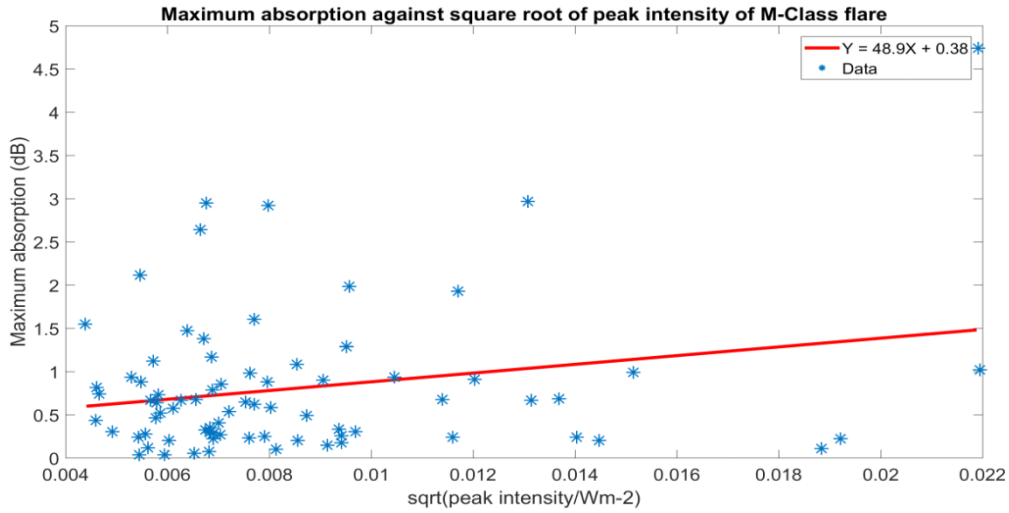


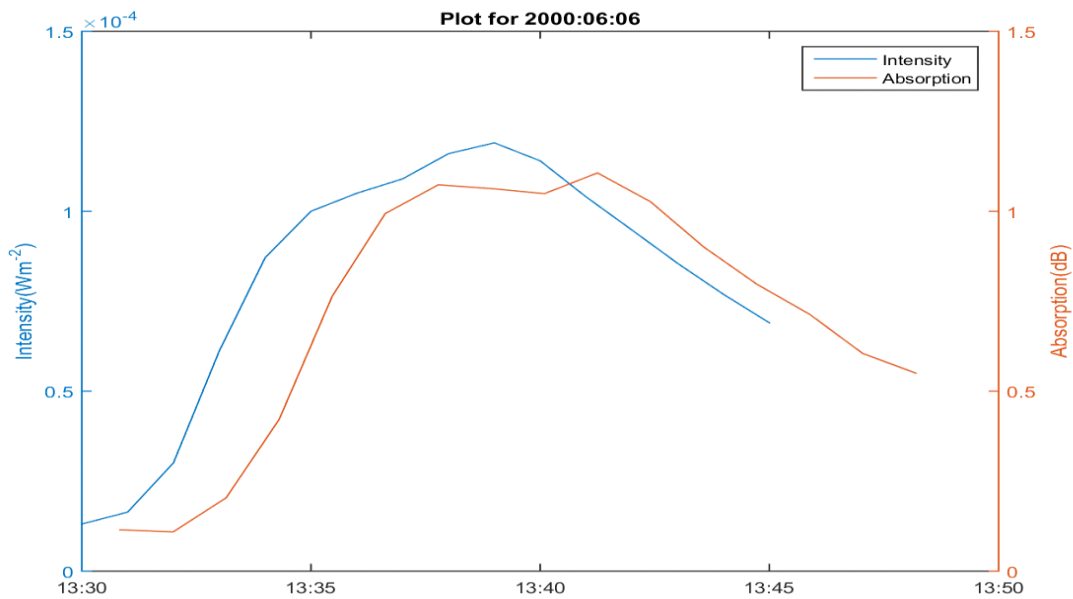
Figure 8: Plot of maximum absorption (dB) vs. square root of maximum flare intensity (Wm^{-2}), Top panel show M-class relation, bottom panel shows X-class relation.

Table 3: Equation of fits for parameters of absorption and flare.

Class of event	Relation for rise time of absorption and rise time of flare intensity	Relation for maximum absorption and peak flare intensity	Relation for decay time of absorption and decay time of flare intensity
M-class flares	Rise time of absorption = 1.32 (Rise time of flare) + 5.97	Maximum absorption = 48.90 (maximum flare intensity) + 0.38	Decay time of absorption = 0.54 (Decay time of flare) + 7.19

X-class flares	Rise time of absorption = $1.22(\text{Rise time of flare}) + 5.05$	Maximum absorption = $32.79(\text{maximum flare intensity}) + 0.30$	Decay time of absorption= $0.31(\text{Decay time of flare}) + 6.29$
----------------	---	--	--

In Table 3, we show linear relations between the rise time of absorption and the rise time of flare; the decay time of absorption from point of maximum absorption and decay time of flare from point of maximum flare intensity. We also show the relation between maximum absorption and the square root of the intensity of flare. Figure 9 shows typical absorption and flare profiles.



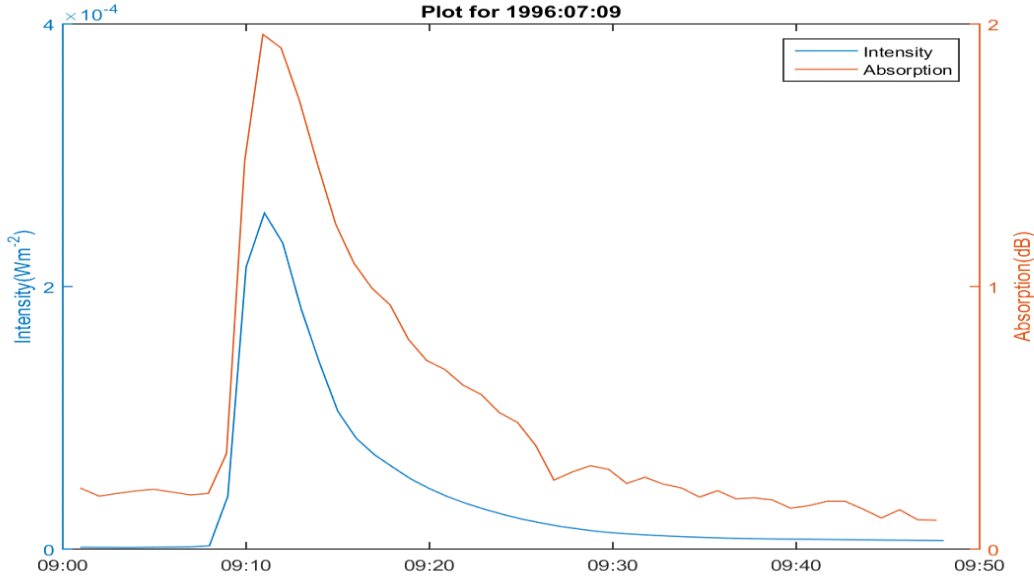


Figure 9: Typical relationship between absorption (dB) and flare intensity (Wm^{-2}) for M-class flare event (upper panel-6th June 2000) and an X-class event (lower panel- 9th July 1996).

The profiles mostly follow an exponential rise and exponential decay from points of maximum absorption and maximum flare intensity. Equation 1 shows the exponential rise relation; equation 2 shows the exponential decay from maximum point while equation 3 provides the relationship between flare and absorption for the duration of the event by combining equations 1 and 2.

$$(1)$$

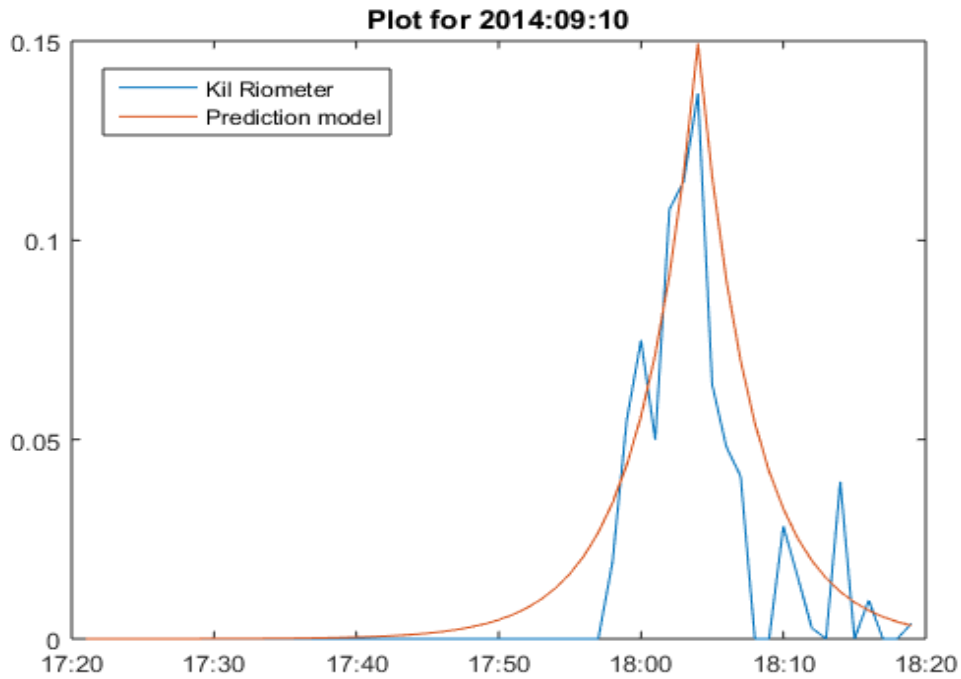
$$\text{Exponential decay} = Ae^{-t/\tau_2} \quad (2)$$

$$\text{Exp rise} + \text{Exp decay} = Ae^{t/\tau_1} + Ae^{-t/\tau_2} \quad (3)$$

5. Analysis and Observations

We observed that there is no significant increase in the maximum absorption recorded during events up to M4 class flares (intensity of $4 \times 10^{-5} \text{ Wm}^{-2}$). Beyond this, there is a noticeable increase in maximum absorption as flare intensity increases. This suggests that flare events below class M4 do not cause significant absorption in the ionosphere. This is likely because the increase in X-ray and UV flux does not cause sufficient ionisation to produce a measurable change in absorption (i.e. below the 0.5dB threshold). The flare induced absorption model produced for M and X-class flares provides a basis for a nowcast of absorption associated with M and X-class events. The model is based on the relational equations derived from (1) flare rise time and rise time in absorption (2) maximum absorption and the square root of peak intensity of flare and (3) decay time of flare and the decay time of absorption integrated into equations 1 and 2. The model result compares better with measured absorption when the peak absorption and

peak intensity occur at almost the same time (± 2 minutes) the correlation on such events is $R=0.89$ whereas for events that has more than ± 2 minutes delay in the peaks of absorption and flare intensity, the $R=0.67$. However, over 90 percent of event analysed have their peak intensity and peak absorption occurring within ± 2 minutes (see Figure 11). In Figure 10 we show typical examples of measured vs. modelled result of absorption induced by solar flare.



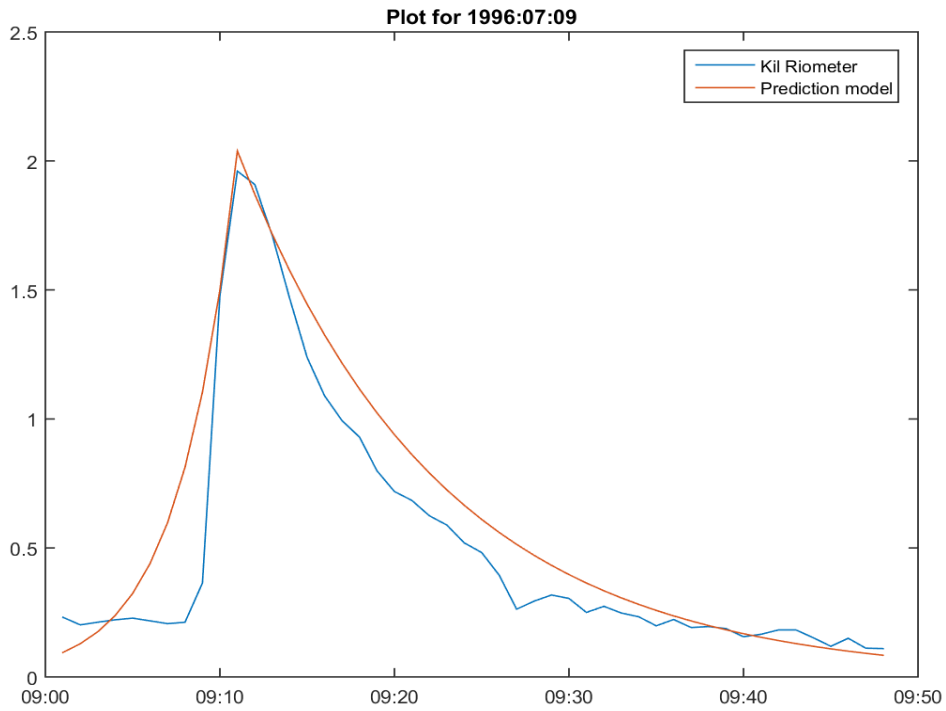


Figure 10: Kilpisjarvi riometer measured absorption (Kil) vs. flare induced modelled absorption (prediction model) for M4.5 flare of 10th September 2014 (upper panel) and 9th July 1996 (bottom panel). The Y-axis shows the absorption (dB) while the X-axis show local time occurrence of flare events.

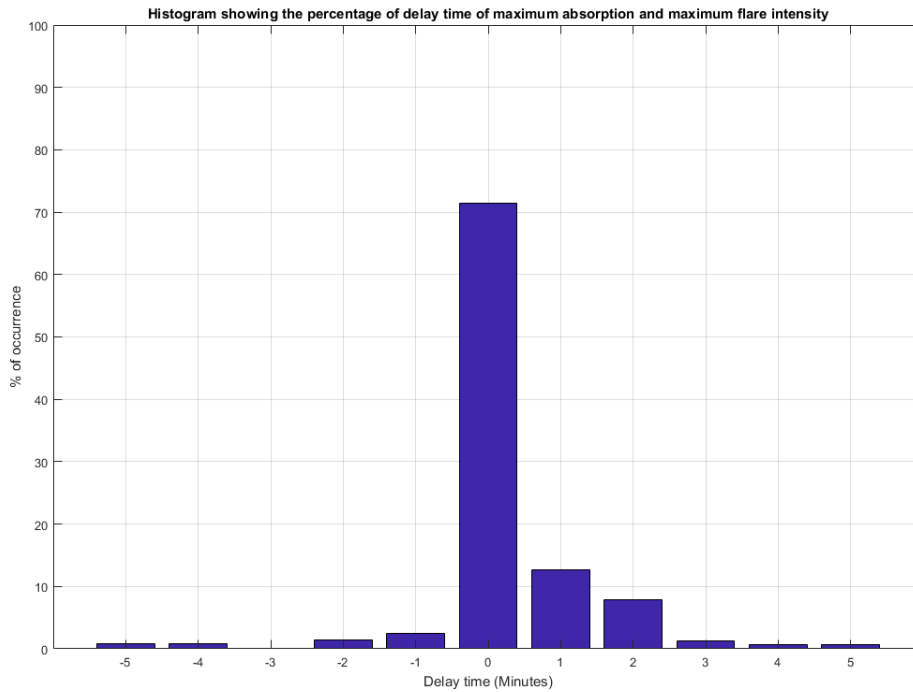


Figure 11: Histogram showing the percentage of occurrence of time delay between maximum absorption and peak intensity of flare. On the time axis, typical time delay is ± 5 minutes. Over 70% of events have their maximum absorption and peak intensity occurring at the same time and over 90% of events occur within ± 2 minutes.

6. Conclusion

For solar flare induced absorption, low intensity flares (C-class flares) do not cause any significant absorption, whereas flares with higher intensity (M and X-class) do. X-class flares having the highest intensity bear the most significant effect on absorption.

A relation between the rise time of absorption and the intensity of the flare producing the absorption was established. Relationships between rise time of absorption and rise time of intensity as well as between maximum absorption and the square root of the maximum flare intensity is presented. In addition, a relation for the relaxation time of flare from the point of maximum intensity and the decay in absorption from maximum absorption is presented. The three relations were used in specifying a flare induced absorption model. An exponential rise and decay model is used to specify the magnitude of absorption induced by solar flare.

REFERENCES

- Bamford R.A, Honary F, Tao H, Vastberg A , Barclay L, (1995). First results from a combined riometer and oblique sounder campaign in the auroral region, IEE National Conference on Antennas and Propagation, 1999 p. 356 – 358.
- Browne S. J, Hargreaves J.K, and Honary B, (1995). An imaging riometer for ionospheric studies, *Electron. Commun. Eng. J.7 (5)*, 209–217.
- Contreira D, Rodrigues F. S, Makita K, and Brum C. G., (2005). An experiment to study solar flare effects on radio-communication signals, *Advances in Space Research*, volume 36, issue 12, pages 2455–2459.
- Hargreaves, J. K. (1995). *Solar terrestrial environment*, Cambridge University Press.
- Hudson H. S. (2011), Global properties of solar flares, *Space Science Reviews*, volume 158, issue 5, pages 5–41.
- Hultqvist B, (1999). *Magnetospheric plasma sources and losses: Final report of the ISSI study project on source and loss processes of magnetospheric plasma*, volume 6, Springer Science & Business Media, ISBN: 978-94-011-4477-3.
- Kavanagh A.J, Kosch M.J, Honary F, Marple S.R, Woodfield E.E and McCrea I.W., (2004). The statistical dependence of auroral absorption on geomagnetic and solar wind parameters, *Annales Geophysicae*, vol.22, pages 877-887.
- Keith T. S. (1991). Observations from the Solar Maximum Mission, *Philosophical Transactions of the Royal Society of London: A Mathematical, Physical and Engineering Sciences*, volume 336, pages 326–337.
- Longden N, Honary F, Kavanagh A. J, and Manninen J, (2007). The driving mechanisms of particle precipitation during moderate geomagnetic storm of 7 January 2005, *Annales Geophysicae*, volume 25, pages 2053–2068.
- Nwankwo V.U.J, Chakrabarti S.K, Ogunmodimu O (2016), Probing geomagnetic storm-driven magnetosphere-ionosphere dynamics in the D-region via propagation characteristics of very low frequency radio signals. *JASTP*, vol.145, pp 154-169.
- Schunk R and Nagy A. (2009). *Ionospheres: physics, plasma physics and chemistry*, Cambridge University press, ISBN-13: 978-0521877060.
- Stauning P. (1996). Investigations of ionospheric radio wave absorption processes using imaging riometer techniques, *Journal of Atmospheric and Terrestrial Physics*, volume 58, no. 6, pages 753–764.
- Tanaka Y, Ishii M, Kubota M, Murayama Y, Mori H and Dirk L, (2007). *Journal of the National Institute of Information and Communications Technology* Vol.54 Nos.1/2.